ChemPubSoc Europe

DOI: 10.1002/ejic.201501469

EurJIC European Journal of Inorganic Chemistry

Full Paper

Metallonucleases

Photoinduced and Self-Activated Nuclease Activity of Copper(II) Complexes with *N*-(Quinolin-8-yl)quinolin-8-sulfonamide – DNA and Bovine Serum Albumin Binding

Alejandro Pascual-Álvarez,[a] Tamara Topala,[a,b] Francisco Estevan,[c] Francisca Sanz,[d] and Gloria Alzuet-Piña*[a]

Dedicated to Professor Joaquín Borrás on occasion of his 70th birthday

Abstract: Two Cu^{II} complexes with a new quinoline sulfonamide derivative and phenanthroline (phen), [Cu(QSQ)(phen)]ClO_4·0.5H_2O (**1**) and [Cu(QSQ)(phen)(H_2O)]ClO_4 (**2**) [HQSQ = *N*-(quinolin-8-yl)quinolin-8-sulfonamide], have been synthesized and physicochemically characterized. Single-crystal X-ray diffraction studies have revealed a highly distorted trigonal-bipyramidal structure for **1** (τ = 0.68) and an almost perfect trigonal-bipyramidal geometry for **2** (τ = 0.92). DNA binding studies, which were performed by thermal denaturation, viscometry, fluorescence spectroscopy, and cyclic voltammetry, indicated a partial intercalation of **1** with $K_{app} = 2.45 \times 10^6$ M^{-1}. The nuclease activity of **1** was investigated upon photoirradiation, with ascorbate/H_2O_2 as the activating agent, and also in the absence of any external reagent. In all cases, **1** was able to perform DNA cleavage, and its nuclease efficiency varied in the order ascorbate/H_2O_2 > photoirradiation > without external cofactors. Mechanistic investigations suggest an oxidative cleavage of DNA involving reactive oxygen species (ROS). The protein binding ability of **1** was also studied with bovine serum albumin (BSA) as a model protein.

Introduction

The interactions of metal complexes with DNA and transition-metal-complex-mediated DNA damage are important areas of chemical research because of their applications in nucleic acid chemistry and cancer research.[1,2] Metal complexes provide highly versatile platforms for drug design. The metal and its oxidation states can be varied, and metal ions also have a range of geometries and coordination numbers that allow the fine-tuning of their chemical reactivity. In addition to the metal center, the ligands can also play important roles in biological activity ranging from recognition of the target site to the activity of any released ligands and ligand-centered redox processes.[3] Since the bis(phenanthroline) copper complex $[Cu(phen)_2]^{2+}$ was first reported as an effective DNA cleaving agent,[4] copper-based chemical nucleases have received special attention.[5] Metal-mediated DNA cleavage can be oxidative at the sugar or the nucleobase as well as hydrolytic at the phosphodiester backbone of DNA. Metal hydrolases tend to show low cleaving efficiency; thus, synthetic chemical nucleases that exhibit oxidative activity are the main focus of the majority of studies on artificial DNAases.[6] Redox-active metallonucleases require the addition of external reagents (oxidizing or reducing agents) or light to produce reactive oxygen species (ROS) such as singlet oxygen or hydroxyl radicals, which ultimately cleave DNA. Among these artificial nucleases, those that can be activated upon irradiation have gained importance in the photodynamic therapy (PDT) of cancer.[7–9] The great advantages of this therapy are its noninvasive nature and its high selectivity, which avoids the significant side-effects of most cytotoxic drugs.[10–14] Although the DNA photocleavage activities of a large number of complexes containing 4d or 5d metals have been studied extensively,[15] the chemistry of copper-based photonucleases is much more unexplored.[16] Recently, diverse strategies have been developed to obtain Cu^{II} complexes that can induce DNA photocleavage. A series of Cu^{II} polypyridyl compounds have been designed with DNA photocleavage activity,[17–21] and ternary Cu^{II} complexes with DNA-binder phenanthroline bases and a photoactive ligand have also been prepared to enhance DNA binding and promote DNA cleavage activity.[16,22]

More recently, copper(II) complexes possessing inherently diverse structural and redox properties have become attractive

[a] *Departament de Química Inorgànica, Facultat de Farmàcia, Universitat de València, 46100 Burjassot (Valencia), Spain*
E-mail: gloria.alzuet@uv.es
http://www.uv.es/
[b] *Department of General and Inorganic Chemistry, Faculty of Pharmacy, UMF Iuliu Haţieganu, Cluj-Napoca, Romania*
[c] *Departament de Química Inorgànica, Facultat de Química, Universitat de València, 46100 Burjassot (Valencia) Spain*
[d] *Servicio de Difracción de Rayos X, Facultad de Ciencias Químicas, Universidad de Salamanca, 37007 Salamanca, Spain*

Supporting information and ORCID(s) from the author(s) for this article are available on the WWW under http://dx.doi.org/10.1002/ejic.201501469.

agents for DNA cleavage owing to their potential self-activating nuclease activity.[5,23–31] Although the detailed cleavage mechanisms of these systems remain unclear, in general, redox reactions involving the ligand and the metal ion seem to initiate DNA cleavage. As pharmaceutical agents, these oxidative cleavers present a larger number of applications in vivo.[5] The search for simple, synthetic metal complexes that bind and cleave DNA by a self-activating mechanism is a real challenge.

In the context of developing metal-based therapeutics, there is a great interest today in the analysis of drug–protein interactions, which greatly influence the absorption, distribution, metabolism, and excretion properties of drugs. Serum albumins (SAs), as the most abundant proteins in the circulatory system, act as transporters and disposers of many endogenous and exogenous compounds.[32,33] The study of the interactions of small molecules with these plasma proteins provides understanding of drug pharmacokinetics and structure–activity relationships. Therefore, studies on the interactions of copper(II) complexes with SA can be useful in the design of antitumoral metal-based therapeutics.[34]

Sulfonamides are appropriate ligands for the preparation of coordination compounds with biological activity, as they possess bactericidal, antiviral, antidiabetic, and diuretic properties,[35–40] and some sulfonamide compounds are under clinical evaluation for cancer treatment. As antitumor agents, sulfonamides can act through a variety of mechanisms such as cell-cycle perturbation, disruption of microtubule assembly, angiogenesis inhibition, and functional suppression of the transcriptional activator NF-V.[41–45] Recently, sulfonamide derivatives bearing biologically active quinoline moieties have shown remarkable in vitro anticancer activity.[46,47] In recent years, our group has reported the prominent oxidative nuclease activity of copper sulfonamide complexes.[48–57] Among these compounds, $[Cu(NST)_2(phen)]$ [HNST = *N*-2-(4,5-dimethylthiazol)naphthalenesulfonamide] was found to induce DNA cleavage upon photoirradiation.[48] Moreover, some of these compounds are potential antitumoral agents that produce cell death by apoptosis.[48–50]

In this work, we report the synthesis and physicochemical characterization of two new copper sulfonamide complexes, $[Cu(QSQ)(phen)]ClO_4·0.5H_2O$ (**1**) and $[Cu(QSQ)(phen)(H_2O)]ClO_4$ (**2**) [HQSQ = *N*-(quinolin-8-yl)quinolin-8-sulfonamide]. The HQSQ ligand bears two quinoline moieties and has been designed to improve the binding ability of the complexes towards DNA. The propensity for DNA binding and the nuclease activity of **1** under different experimental conditions have been studied in detail. Complex **1** is not only an efficient photonuclease but also the first example of a Cu sulfonamide complex that can promote DNA cleavage by a self-activating mechanism. Finally, the binding of **1** to bovine serum albumin (BSA), as a model protein, has been evaluated.

Results and Discussion

The HQSQ ligand, **1**, and **2** were prepared according to Scheme 1.

The sulfonamide and the ternary complexes showed good solubility in dimethyl sulfoxide (DMSO) and *N*,*N*-dimethylformamide (DMF) and low solubility in aqueous media. They were stable in solution. The peak at m/z = 577 in the ESI+ mass spectra of the complexes, assigned to $[Cu(QSQ)(phen)]^+$, indicates the stability of the ternary structures in solution.

X-ray Crystallography and Spectroscopic Properties

ORTEP perspective views of **1** and **2** are shown in Figures 1 and 2, respectively. Selected bond lengths and angles are listed in Table 1.

The crystal structures of the compounds consist of discrete monomeric Cu^{II} cations with one perchlorate anion. In both complexes, the Cu^{II} center is pentacoordinated. In **1**, the Cu^{II} center is coordinated by five nitrogen atoms, that is, the two N atoms [N(4) and N(5)] from the phenanthroline ligand and the three nitrogen atoms [N(1), N(2), and N(3)] of the sulfonamide derivative. In **2**, the metal ion is surrounded by the two N atoms [N(4) and N(5)] from the phenanthroline molecule, two N atoms [N(2) and N(3)] of the sulfonamide ligand, and the oxygen atom [O(3)] of a water molecule. The coordination geometries of the Cu^{II} centers in both complexes can be described as distorted trigonal bipyramidal according to the Addison–Reedijk geometric criterion,[58] in which the parameter τ is calculated from the

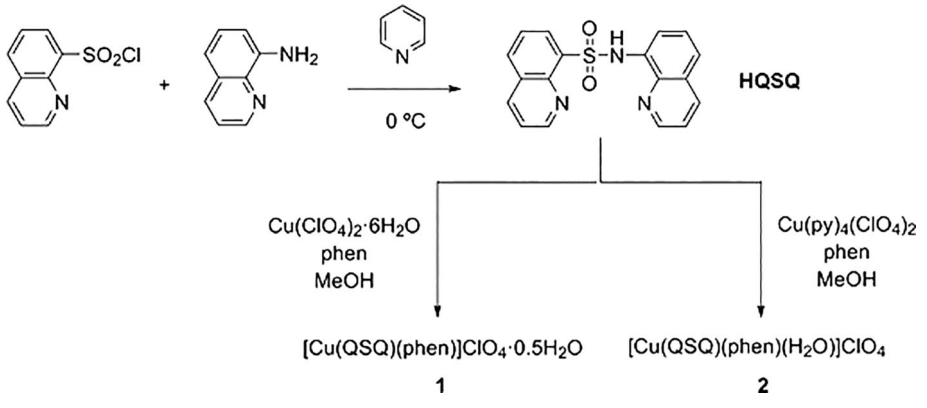

Scheme 1. Synthesis of *N*-(quinolin-8-yl)quinolin-8-sulfonamide (HQSQ) and complexes **1** and **2**.

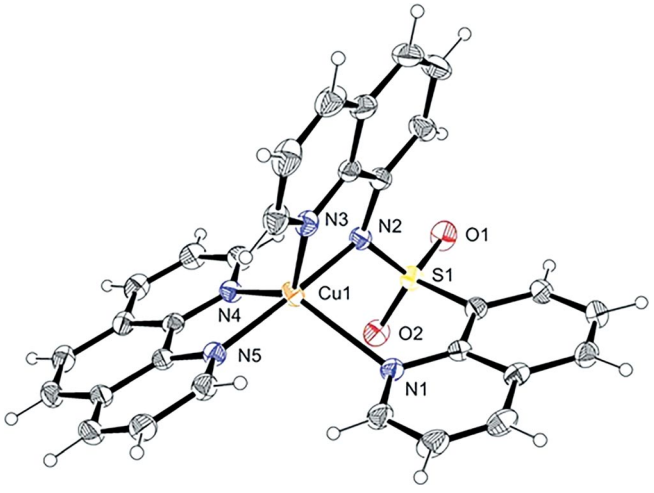

Figure 1. ORTEP drawing of **1**. The perchlorate anion and the water molecule are omitted for clarity.

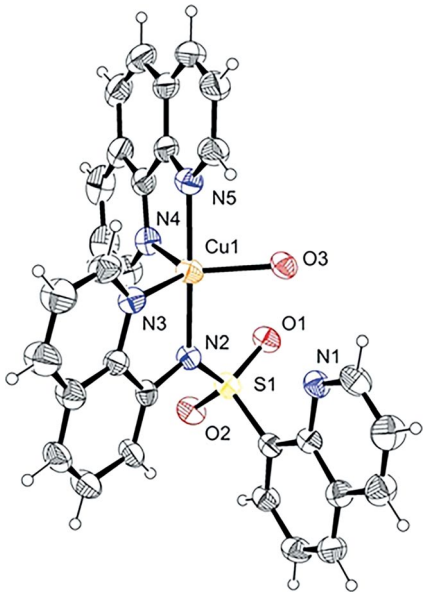

Figure 2. ORTEP drawing of **2**. The perchlorate anion is omitted for clarity.

Table 1. Selected bond lengths [Å] and angles [°].

[Cu(QSQ)(phen)]ClO_4·0.5H_2O (**1**)		[Cu(QSQ)(phen)(H_2O)]ClO_4 (**2**)	
Cu(1)–N(5)	2.024(2)	Cu(1)–N(2)	1.961(5)
Cu(1)–N(4)	2.042(2)	Cu(1)–N(5)	1.999(5)
Cu(1)–N(2)	1.941(2)	Cu(1)–N(3)	2.038(5)
Cu(1)–N(3)	2.053(2)	Cu(1)–O(3)	2.085(4)
Cu(1)–N(1)	2.479(2)	Cu(1)–N(4)	2.106(5)
N(2)–Cu(1)–N(5)	174.63(9)	N(2)–Cu(1)–N(5)	177.7(2)
N(2)–Cu(1)–N(4)	93.55(9)	N(2)–Cu(1)–N(3)	81.87(19)
N(5)–Cu(1)–N(4)	81.08(9)	N(5)–Cu(1)–N(3)	99.0(2)
N(2)–Cu(1)–N(3)	82.70(10)	N(2)–Cu(1)–O(3)	95.76(18)
N(5)–Cu(1)–N(3)	100.87(10)	N(5)–Cu(1)–O(3)	85.6(2)
N(4)–Cu(1)–N(3)	130.99(10)	N(3)–Cu(1)–O(3)	121.75(19)
N(2)–Cu(1)–N(1)	85.15(9)	N(2)–Cu(1)–N(4)	97.3(2)
N(5)–Cu(1)–N(1)	98.49(9)	N(5)–Cu(1)–N(4)	80.5(2)
N(4)–Cu(1)–N(1)	133.94(9)	N(3)–Cu(1)–N(4)	115.6(2)
N(3)–Cu(1)–N(1)	94.60(9)	O(3)–Cu(1)–N(4)	122.35(19)

observed L–M–L′ basal angles and is an index of the degree of trigonality of the structure that ranges from zero for a perfect square pyramid to unity for a perfect trigonal bipyramid. The τ values of 0.68 and 0.92 for **1** and **2**, respectively, reflect that the five-coordinate geometries around the Cu^{II} centers are very distorted trigonal bipyramidal for **1** and almost perfect trigonal bipyramidal for **2**. The basal plane in **1** is formed by one N atom [N(4)] of the phenanthroline molecule and the two quinoline nitrogen atoms [N(1) and N(3)] belonging to the sulfonamide derivative, whereas the equatorial positions in **2** are occupied by one N atom of the phenanthroline ligand [N(4)], the quinoline N atom [N(3)] of the sulfonamide ligand, and the water oxygen atom [O(3)]. In both compounds, the apical positions are occupied by the sulfonamido nitrogen atom [N(2)] and one phenanthroline nitrogen atom [N(5)]. The Cu–N bond lengths range from 1.941(2) to 2.479(2) and from 1.961(5) to 2.106(5) Å in **1** and **2**, respectively. The Cu–$N_{quinoline}$ bond lengths are slightly longer than those described for Cu^{II} complexes with bis(8-aminoquinoline) ligands.[59] The Cu–$N_{sulfonamide}$ and the Cu–N_{phen} bond lengths are normal lengths, similar to those found in related ternary copper(II) sulfonamide phenanthroline compounds.[48,50] Notably, in **1**, in which the sulfonamide acts as a tridentate ligand, the coordination angles and the rather long Cu–N(1) bond length reflect the strong distortion caused by the steric hindrance of the sulfonamide derivative.

The crystal structure of **1** is stabilized by the presence of intermolecular π–π interactions between the central rings of two phenanthroline molecules in adjacent units. These rings are stacked with a centroid–centroid distance of 3.744 Å and a dihedral angle of 0° (Figure S1a).

Compound **2** is stabilized by intermolecular stacking interactions between the C_6 quinoline ring and the central phenanthroline ring of two different units with a centroid–centroid distance of 3.769 Å and a dihedral angle between the planes of 12.32° (Figure S1b).

The two complexes present very similar IR spectra. Compared with the spectrum of the free ligand, the most remarkable changes occur in the characteristic bands corresponding to the sulfonamide group. Thus, the band at $\tilde{\nu}$ = 3168 cm^{-1}, assigned to the ν(N–H) vibration in the free ligand, is not found in the IR spectra of the compounds as a consequence of the deprotonation of the sulfonamide derivative upon coordination. The $\nu_{as}(SO_2)$ and $\nu_s(SO_2)$ vibrations are shifted to lower frequencies, and the ν(S–N) vibration shifts to higher frequency (by ca. 30 cm^{-1}) with respect to the corresponding bands of the free ligand. Considering the different coordination behavior of QSQ^- in the compounds (tridentate in **1** and bidentate in **2**), these modifications are probably not related to the coordination itself but to the deprotonation of the sulfonamide group. In addition, the spectra of the complexes exhibit bands at $\tilde{\nu}$ = 1522 and 850 cm^{-1}, which are assigned to the characteristic vibrations of coordinated phenanthroline.[60] The strong band at $\tilde{\nu} \approx 1077$ cm^{-1} can be attributed to the uncoordinated perchlorate ion.[61]

Both complexes have axial polycrystalline X-band electron paramagnetic resonance (EPR) spectra at room temperature (Figure S2). The EPR parameters calculated through simula-

tion[62] are $g_{\parallel}$ = 2.240, $g_{\perp}$ = 2.082 for **1** and $g_{\parallel}$ = 2.210, $g_{\perp}$ = 2.085 for **2**.

The X-band EPR spectra of both complexes in frozen DMF solution are axial with resolved hyperfine structures due to the copper center (S = 1/2 and I = 3/2) in the parallel region. Both EPR spectra are almost coincident (Figure S3) and have essentially identical EPR parameters ($g_{\parallel}$ = 2.250, $g_{\perp}$ = 2.080, and $A_{\parallel}$ = 135 × 10^{-4} cm^{-1}); this indicates that the compounds adopt the same structure in solution.[63] A mainly $d_{x^2-y^2}$ orbital ground state is suggested by $g_{\parallel} > g_{\perp}$, and the calculated $A_{\parallel}$ values for **1** and **2** are consistent with the presence of a C_{4v} (square-pyramidal) geometry.[64] Notably, the frozen EPR spectra of both complexes show a dominantly tetragonal component in the solution stereochemistry; especially for **1**, this could mean a change from an almost regular trigonal-bipyramidal geometry towards a more square-pyramidal one.[58]

The electronic spectra of **1** and **2** in DMF solution exhibit a broad ligand-field band centered at $\lambda \approx 700$ nm with a weak low-energy shoulder at $\lambda \approx 920$ nm (Figure S4). Both spectra are indicative of a pentacoordinate geometry.[65,66] The $d_{x^2-y^2}$ ground state, as deduced from the EPR spectra, leads to a tentative assignment of the d–d bands as $d_{x^2-y^2} \rightarrow d_{xz}$, d_{xy}, d_{yz} for the higher-energy band and $d_{x^2-y^2} \rightarrow d_{z^2}$ within the lower-energy envelope.[58] Both spectra also present a shoulder at $\lambda \approx$ 480 nm, which can be attributed to a ligand-to-metal charge-transfer (LMCT) transition between the phenanthroline ligand and the copper(II) ion.[48] The close similarity of the UV/Vis spectra of the two complexes suggests that **1** and **2** present the same chromophore in solution. These results are in good agreement with the EPR results. On the basis of the results derived from the ESI+ MS studies for both compounds, $[Cu(QSQ)(phen)]^+$ is assumed to be the complex entity in solution.

As all of the solution studies support that both **1** and **2** give rise to the same species in solution, we have tested the biological activity of only one of the compounds. For this purpose, we have chosen **1** as it was obtained in a higher yield.

DNA Binding Interactions

DNA binding is a critical step for subsequent DNA cleavage. Therefore, before we investigated the nuclease activity of **1**, we studied its ability to bind to DNA by different techniques.

Thermal Denaturation

The binding of **1** to calf thymus DNA (CT-DNA) was studied by measuring changes in the melting temperature (T_m) of DNA, which characterizes the transition from a double-stranded nucleic acid to a single-stranded one.[52,67] Compound **1** produced an increase in T_m (ΔT_m = 5.2 °C at [DNA]/[complex] = 2; Figure 3), which is indicative of an interaction between DNA and the compound that stabilizes the native DNA conformation. Moreover, the moderate increase in the melting temperature of CT-DNA suggests that **1** presents primarily a groove binding propensity.[49,68]

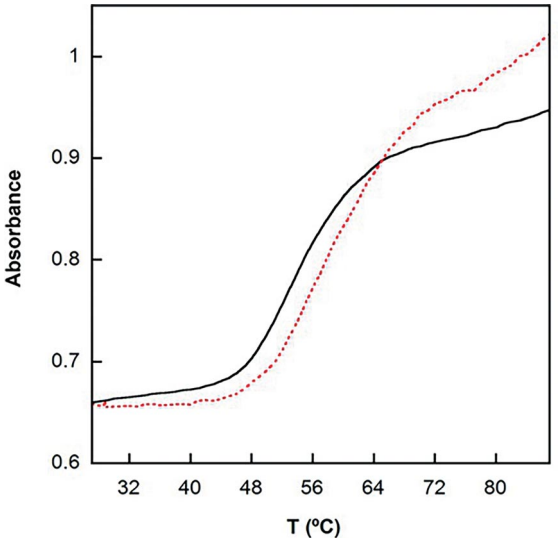

Figure 3. Melting temperature of CT-DNA in the absence (black solid line) and presence of **1** (red dashed line); [DNA] = 100 μM, [complex] = 50 μM, phosphate buffer (1 mM, 2 mM NaCl, pH 7.2), and 2.5 % DMF.

Ethidium Bromide Displacement Assay

Fluorescence spectroscopic studies were also performed to obtain a better understanding of the interaction of the compound with DNA. These studies were performed with ethidium bromide (EB). Ethidium bromide is a planar cationic dye that is used widely as a sensitive fluorescence probe for native DNA. EB emits intense fluorescence in the presence of DNA, and the extent of the fluorescence quenching of EB bound to DNA by the addition of a second molecule gives a measure of its DNA binding propensity. The emission of the DNA–EB adduct after the addition of a second molecule can be quenched through the replacement of EB, the acceptance of the excited-state electron of the EB through a photoelectron transfer mechanism, or both.[69,70] As displayed in Figure 4, the addition of increasing concentrations of **1** to DNA previously treated with EB caused

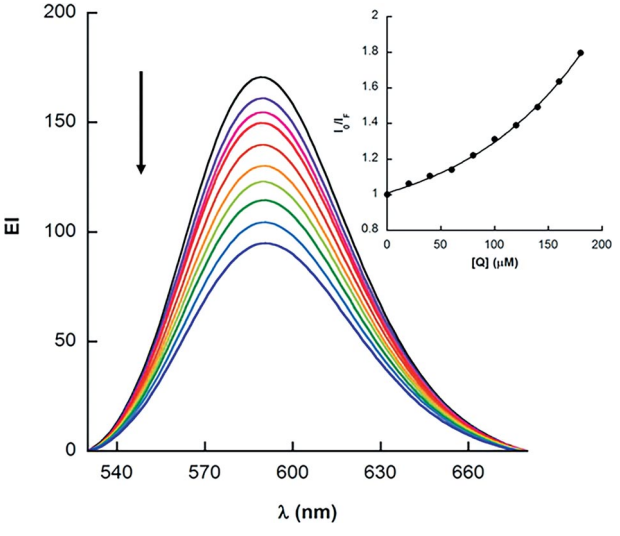

Figure 4. Emission spectra of EB bound to DNA in the absence and presence of 20, 40, 60, 80, 100, 120, 140, 160, 180 μM of **1** in 0.1 M cacodylate buffer (pH 6.0) and 3.5 % DMF. The arrow shows the changes in intensity at increasing concentrations of the complex. Inset: Stern–Volmer plot.

an appreciable reduction in the emission intensity of ca. 45 %, which clearly indicates the higher binding affinity of **1**.

Generally, the fluorescence quenching of EB bound to DNA by the complexes follows the classical linear Stern–Volmer equation, $I_0/I = 1 + K_{SV}[Q]$, in which I_0 and I are the fluorescence intensities of the fluorophore in the absence and presence of quencher, K_{SV} is the Stern–Volmer quenching constant, and [Q] is the quencher concentration. However, in our case a nonlinear, upward-curving Stern–Volmer plot was obtained (inset in Figure 4). Such a difference in the Stern–Volmer plot is consistent with the occurrence of at least two quenching mechanisms, one of which is fast relative to the resolution in the time-resolved experiment (named as static), and a second that is slow relative to this time scale (named as dynamic).[71] The data for **1** follow a compressed exponential growth behavior given by Equation (1) with $a = 0.207$, $b = 115.16$, and $c = 0.803$:[72]

$$I_0/I = a \exp([Q]/b) + c \quad (1)$$

The apparent binding constant (K_{app}) was also calculated from the equation $K_{EB}[EB] = K_{app}[complex]$, in which $K_{EB} = 1.0 \times 10^7$ M^{-1},[73] [EB] = 50 μM, and [complex] is the concentration that causes a 50 % quenching of the initial EB fluorescence (203.4 μM). The calculated K_{app} value for **1** of 2.45×10^6 M^{-1} is similar to those previously reported for related Cu^{II} sulfonamide compounds and indicates that the interaction of **1** with DNA is rather strong.[48,51,54]

Viscosity Studies

To clarify the binding of **1** to DNA, viscosity measurements were performed on CT-DNA with variation of the concentration of the compound. Hydrodynamic measurements that are sensitive to length changes are regarded as the least ambiguous and the most critical tests of a DNA binding model in solution and provide reliable evidence for the DNA binding mode. Our results (Figure 5) reveal that **1** produced an increase in the viscosity of CT-DNA, which indicates an intercalative binding. This increase in viscosity follows a similar pattern to that caused by $[Cu(phen)_2]^{2+}$ and the related sulfonamide compound $[Cu(NST)_2(NH_3)_2]\cdot H_2O$, both of which interact with DNA through partial intercalation.[48] Therefore, the involvement of **1** in partial intercalative interactions with DNA base pairs can be proposed.

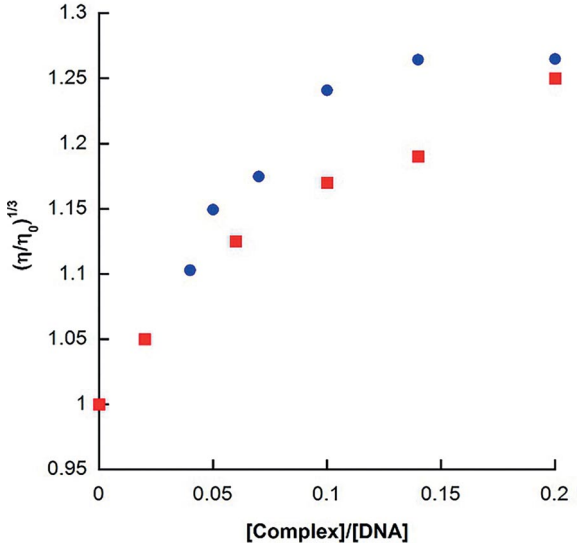

Figure 5. Effect of **1** (blue ●) and $[Cu(phen)_2]^{2+}$ (red ■) on the relative viscosity of CT-DNA in 0.1 M cacodylate buffer (pH 6.0) and 2 % DMF.

Cyclic Voltammetry

The binding of **1** to DNA was also investigated by cyclic voltammetry. The application of electrochemical methods to study the interactions of small molecules with DNA provides a useful complement to spectroscopic methods and may yield information about the binding mode. In general, the electrochemical potential of the complex presents a positive shift when the complex binds to DNA through intercalation, whereas it exhibits a negative shift for an electrostatic interaction between the complex and DNA.[74]

The cyclic voltammogram of **1** in DMF (Figure 6) shows a quasireversible process that corresponds to the reduction of Cu^{II} to Cu^{I} with the cathodic (E_{pc}) and the anodic (E_{pa}) peaks at –0.10 and –0.04 V, respectively. The addition of DNA to **1** results in changes in the voltammogram of **1** that suggest a strong interaction of **1** with DNA. First, a significant decrease of the voltammetric peak currents is due to the slow diffusion of an equilibrium mixture of the free and DNA-bound **1** to the electrode surface.[52] Moreover, the Cu^{II}/Cu^{I} electron-transfer process becomes less reversible in the presence of DNA. On the other hand, the cathodic potential presents a gradual positive shift as the amount of DNA increases, which is in good agreement with the viscosity results and indicates the intercalation of **1** between DNA base pairs.[74,75]

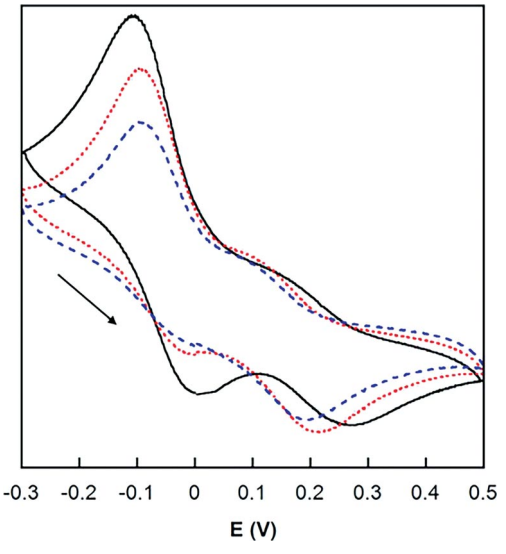

Figure 6. Cyclic voltammograms of **1** in the absence (black solid line) and presence of CT-DNA (red dashed line: [complex]/[DNA] = 10; blue dashed line: [complex]/[DNA] = 20).

DNA Cleavage

The photoinduced DNA cleavage activity of **1** was studied with supercoiled (SC) pUC18 DNA upon irradiation with 365 nm UV-

A light for 2 h, and the results are shown in Figure 7. On the basis of our previous results on Cu^{II} sulfonamide compounds as DNA photocleavers,[48] **1** could be a good candidate for this study because its electronic spectra exhibit an LMCT band close to the photoactivation wavelength. Compound **1** exhibited photonuclease activity, which was dependent on concentration. At 10 and 12.5 μM (Figure 7, lanes 7 and 8) the complex was able to produce a partial conversion of SC-DNA (Form I) into its nicked circular form (Form II). At higher concentrations (15, 17.5, and 20 μM), **1** induced the complete degradation of the supercoiled form to produce ca. 99 % DNA form II and a small quantity (<1 %) of DNA form I (Figure 7, lanes 9–11). Copper(II) perchlorate (Figure 7, lanes 4 and 5) and HQSQ (Figure 7, lanes 14–15) are individually cleavage inactive upon irradiation under the same experimental conditions. Therefore, the involvement of the metal center seems to be apparent in the metal-assisted DNA cleavage reaction, which involves the LMCT band, as was found for the related [Cu(NST)$_2$(phen)].[48]

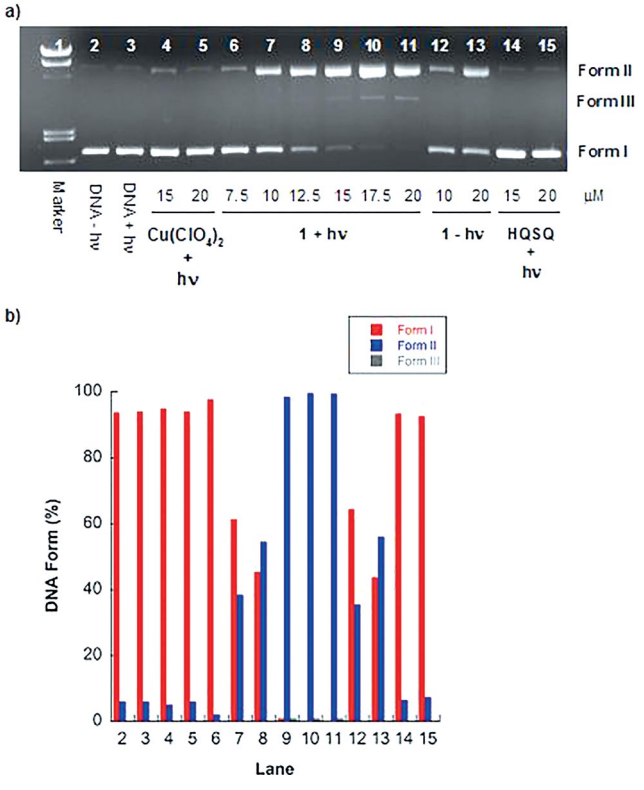

Figure 7. (a) Agarose gel electrophoresis of pUC18 plasmid DNA (37.5 μM bp) treated with **1** upon irradiation with UV-A light. Incubation time 2 h (37 °C); (b) Quantification data of DNA forms. Lanes: (1) λDNA/EcoR1 + HindIII marker, (2) pUC18 control without irradiation, (3) pUC18 control, (4) $Cu(ClO_4)_2$ 15 μM, (5) $Cu(ClO_4)_2$ 20 μM, (6) **1** 7.5 μM, (7) **1** 10 μM, (8) **1** 12.5 μM, (9) **1** 15 μM, (10) **1** 17.5 μM, (11) **1** 20 μM, (12) **1** 10 μM without irradiation, (13) **1** 20 μM without irradiation, (14) HQSQ 15 μM, (15) HQSQ 20 μM.

In an oxygen atmosphere, DNA photocleavage can proceed through two major mechanistic pathways (Scheme 2).[10] In a type II process, the excited electronic state of the complex through efficient intersystem crossing (ISC) could generate an excited state that could activate molecular oxygen to its reactive singlet state ($^1O_2$) by energy transfer. In an alternate pathway, type I, the redox-active photoactivated complex can reduce molecular oxygen to generate reactive hydroxyl radical species by a photoredox mechanism.[76]

The mechanistic pathways involved in the photocleavage reactions were investigated with different ROS scavengers (Figure 8). Sodium formate and KI were employed as hydroxyl radical scavengers, disodium 4,5-dihydroxy-1,3-benzenedisulfonate (tiron) was employed as a superoxide radical scavenger, and 1,4-diazabicyclo[2,2,2]octane (DABCO) and 2,2,6,6-tetramethyl-4-piperidone (TMPP) were employed as $^1O_2$ scavengers. Also, D_2O was used as a detector of singlet oxygen formation, as the lifetime of singlet oxygen is significantly longer in D_2O than in H_2O.

The possibility of a type II singlet oxygen pathway can be ruled out as singlet oxygen scavengers (DABCO and TMPP; Figure 8, lanes 7 and 8, respectively) and D_2O (Figure 8, lane 9) showed no apparent effects on the DNA cleavage activity. The addition of sodium formate and, in particular, KI (Figure 8, lanes 5 and 6, respectively) attenuated the photoactivity of the compound significantly; this, suggests that hydroxyl radicals are involved in the photocleavage reaction. The superoxide quencher tiron (Figure 8, lane 10) also clearly inhibits the cleavage activity, which indicates the participation of superoxide in the DNA damage mediated by the compound. In the presence of neocuproine (Figure 8, lane 11), DNA degradation is also diminished, which suggests the reduction of the Cu^{II} to Cu^{I} during the DNA cleavage process.

All of these results together clearly seem to indicate a photoredox pathway in which the Cu^{II} compound gives rise to reactive Cu^{I} species with the subsequent generation of hydroxyl and superoxide radicals, which are the active species involved in the DNA cleavage, in a similar mechanistic pathway to that proposed for the previously reported [Cu(NST)$_2$(phen)].[48]

Notably, as seen in lanes 12 and 13 of Figure 7, the complex is able to produce a partial SC-DNA degradation without photoirradiation. This finding can be of great relevance because it

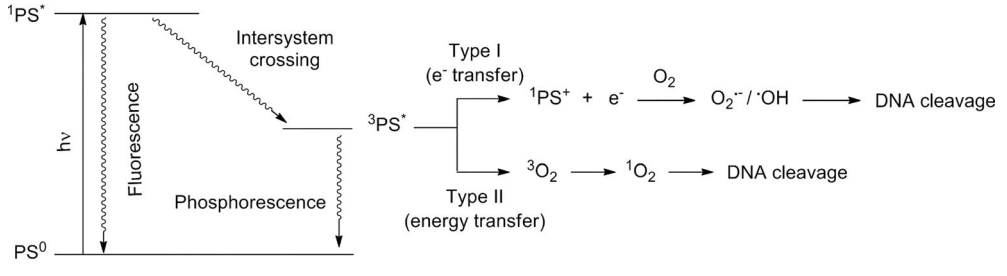

Scheme 2. General DNA photocleavage mechanism.

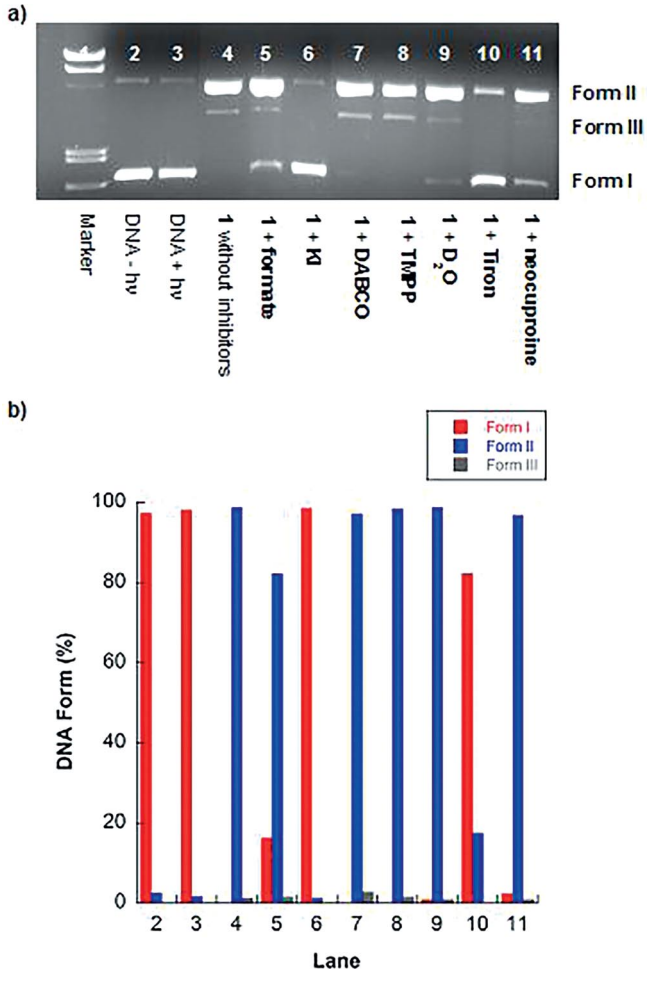

Figure 8. (a) Agarose gel electrophoresis of pUC18 plasmid DNA (37.5 μM bp) treated with **1** (20 μM) upon irradiation under UV-A light in the presence of potential inhibitors. Incubation time 2 h (37 °C). (b) Quantification data of DNA forms. Lanes: (1) λDNA/EcoR1 + HindIII marker, (2) pUC18 control without irradiation, (3) pUC18 control, (4) **1** without inhibitors, (5) sodium formate (0.4 M), (6) KI (0.4 M), (7) DABCO (0.4 M), (8) TMPP (0.4 M), (9) D_2O, (10) tiron (10 mM), (11) neocuproine (40 μM).

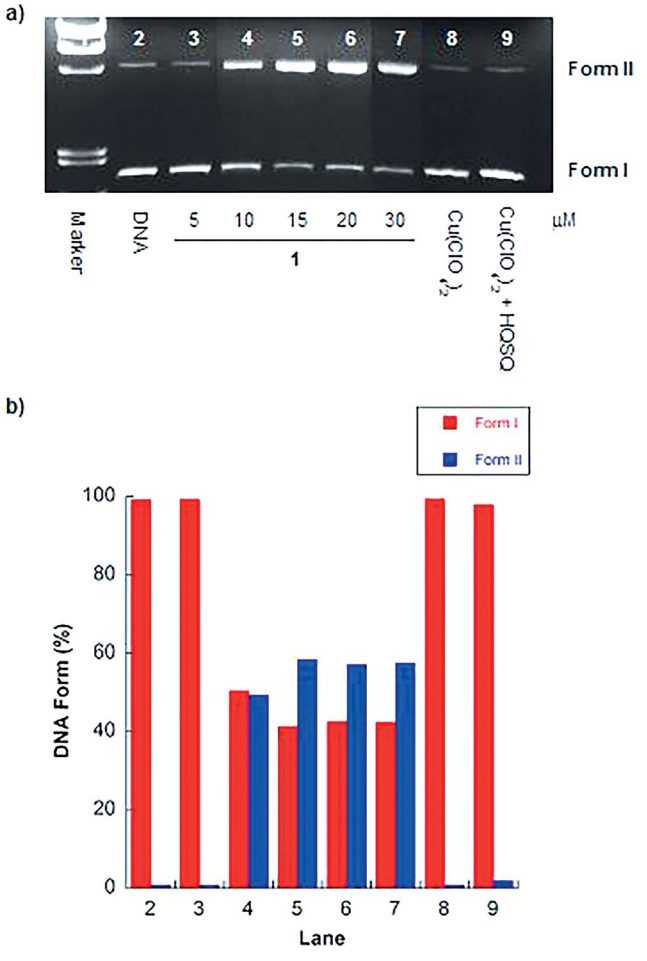

Figure 9. (a) Agarose gel electrophoresis of pUC18 plasmid DNA (37.5 μM bp) treated with **1** without activator. Incubation time 2 h (37 °C); (b) Quantification data of DNA forms. Lanes: (1) λDNA/EcoR1 + HindIII marker, (2) pUC18 control, (3) **1** 5 μM, (4) **1** 10 μM, (5) **1** 15 μM, (6) **1** 20 μM, (7) **1** 30 μM, (8) $Cu(ClO_4)_2$ 30 μM, (9) $Cu(ClO_4)_2$ + HQSQ 30 μM.

could mean that **1** is able to mediate DNA cleavage through self-activation. Therefore, we decided to explore the cleavage of plasmid pUC18 induced by **1** in more detail in the absence of external cofactors (Figure 9). Except for a concentration of 5 μM (Figure 9, lane 3), **1** promoted the partial cleavage of plasmid pUC18 from the SC form I to the nicked circular (NC) form II. At 10 and 15 μM, ca. 50 and 58 % of SC-DNA is transformed into NC DNA (Figure 9, lanes 4 and 5). However, the cleavage efficiency (ca. 58 % Form II) was not enhanced at higher concentrations (20 and 30 μM; Figure 9, lanes 6 and 7). No cleavage was observed for Cu^{II} alone (Figure 9, lane 8) or for the control in which equimolar amounts of Cu^{II} and HQSQ were added to the reaction mixture (Figure 9, lane 9).

Investigations of the cleavage mechanism are highly interesting for copper complexes that exhibit nuclease activity in the absence of any external reagent. Self-activated DNA cleavage can occur by hydrolytic or oxidative pathways. In the first case, the nuclease activity is not inhibited by radical scavengers, whereas the DNA damage in the second case is inhibited by radical scavengers owing to the involvement of reactive oxygen species in the DNA breakdown. In the search for a mechanism, the nuclease activity of **1** without external activating agents was evaluated in the presence of different radical scavengers and in the presence of the Cu^{I} chelator neocuproine (Figure 10).

The hydroxyl radical scavengers sodium formate and KI (Figure 10, lanes 4 and 5) decreased the cleavage activity of **1** significantly; this indicates that hydroxyl radicals are involved in the scission process. Also, the superoxide radical scavenger tiron blocked the DNA cleavage (Figure 10, lane 7); therefore, superoxide plays an important role in the nuclease activity of **1**. However, the presence of D_2O has no apparent effect on the DNA cleavage (Figure 10, lane 6), a fact that excludes the involvement of singlet oxygen in the DNA cleavage reaction. Neocuproine reduces DNA strand scission dramatically (Figure 10, lane 8), and this indicates that the reduction of Cu^{II} occurs during the production of the reactive oxygen species. Although the precise details of the mechanism are not well understood, on the basis of the above findings, a cleavage process that involves hydroxyl and superoxide radicals with Cu^{II} reduction, that is a self-activating oxidative pathway, can be pro-

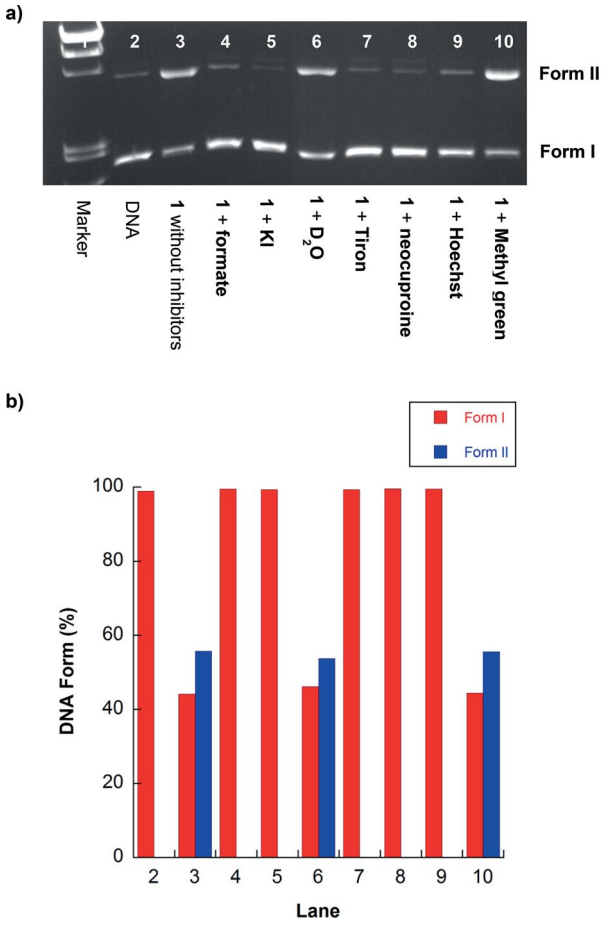

Figure 10. (a) Agarose gel electrophoresis of pUC18 plasmid DNA (37.5 μM bp) treated with **1** (30 μM) without activator in the presence of potential inhibitors. Incubation time 2 h (37 °C). (b) Quantification data of DNA forms. Lanes: (1) λDNA/EcoR1 + HindIII marker, (2) pUC18 control, (3) **1** without inhibitors, (4) sodium formate (0.4 M), (5) KI (0.4 M), (6) D_2O, (7) Tiron (10 mM), (8) neocuproine (60 μM), (9) Hoechst 33258 (8 μM), (10) methyl green (3 μM).

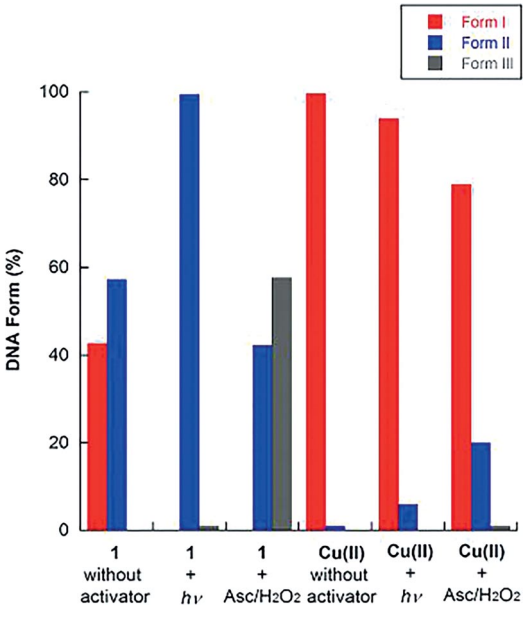

Figure 11. DNA cleavage efficiency mediated by **1** and Cu^{II} under different experimental conditions. Without activator: [**1**] and [Cu^{II}] = 30 μM; upon UV-A irradiation: [**1**] and [Cu^{II}] = 20 μM; in the presence of ascorbate/H_2O_2: [**1**] = 10 μM and [Cu^{II}] = 20 μM.

posed for the DNA cleavage activity of **1**. Interestingly, **1** is the first example of a Cu^{II} sulfonamide compound that exhibits self-oxidative cleavage. This is a promising result, as we have obtained a large number of Cu^{II} sulfonamide complexes as chemical nucleases in recent years,[48–57] but none of them showed nuclease activity without external activating agents.

Furthermore, the DNA groove binding propensity of **1** was studied with Hoechst 33258 as a minor groove binder (Figure 10, lane 9) and methyl green as a major groove binder (Figure 10, lane 10). The addition of **1** to the methyl green bound SC-DNA showed no apparent decrease in the DNA cleavage activity. However, the efficiency of **1** was slightly inhibited by Hoechst-bound SC-DNA; this suggests to some extent that the compound exhibits a minor groove preference.

To get a better insight into the DNA cleavage mediated by **1**, we also studied its nuclease activity under redox conditions by using ascorbate/H_2O_2 as the activating agent. The results (Figure S5) showed that the complex behaves as a very efficient chemical nuclease. In the presence of ascorbate/H_2O_2 (1 equiv.), **1** at concentrations of 10 to 20 μM is able to convert SC-DNA into open circular and linear DNA (Figure S5, lanes 10–13). In particular, the high efficiency of **1** as a chemical nuclease in the presence of ascorbate/H_2O_2 is clearly shown at 20 μM (Figure S5, lane 13). At this concentration, **1** is able to fully transform SC-DNA into ca. 42 % Form II and ca. 58 % Form III. Therefore, the nuclease activity of the compound under redox conditions is increased significantly with respect to that exhibited by **1** in the absence of activators or upon irradiation. Therefore, the activity of the compound follows the order ascorbate/H_2O_2 > photoirradiation > without external agents (see Figure 11).

To understand the difference in the DNA cleavage activity of **1** under the different experimental conditions, we also investigated the DNA cleavage mechanism in the presence of ascorbate/H_2O_2 (Figure S6). Hydroxyl radical scavengers (sodium formate, KI, and DMSO) inhibited the DNA breakdown significantly (Figure S6, lanes 5–7). Thus, it would seem that the cleavage pathway involves the formation of hydroxyl radicals. The DNA strand cleavage is also decreased with tiron (Figure S6, lane 11), which suggests the participation of superoxide, probably through the Haber–Weiss mechanism, in which superoxide reacts with hydrogen peroxide to produce hydroxyl radicals. The singlet oxygen scavengers DABCO (Figure S6, lane 8) and TMPP (Figure S6, lane 9) protect against the DNA strand cleavage induced by the compound; this suggests that $^1O_2$ or singlet oxygen-like species participate in the oxidative cleavage. The involvement of $^1O_2$ is supported by the slight increase in DNA cleavage found when D_2O was added to the reaction mixture (Figure S6, lane 10). The Cu^I chelator, neocuproine (Figure S6, lane 12) diminishes the cleavage mediated by **1**. Therefore, the reduction of the copper(II) complex during the DNA cleavage process can be deduced. According to our results, the generation of a Cu^I complex by ascorbate was expected to lead to the activation of dioxygen, which could, in turn, produce the intermediate or intermediates responsible for plasmid DNA

strand scission. Interestingly, the role of singlet oxygen in the cleavage process mediated by **1** in the presence of ascorbate/H_2O_2 diverges from that observed without activating agents or upon photoirradiation, and this could be, at least in part, the reason for the higher nuclease activity of **1** under redox conditions.

Protein Binding Studies

To study the interactions of **1** with SAs (serum albumins), fluorescence quenching studies with BSA (bovine serum albumin), as a model protein, were performed.

BSA fluorescence is mainly attributed to the presence of three amino acids, namely, tryptophan, tyrosine, and phenylalanine.[77] Protein conformational transitions, subunit associations, substrate binding, or denaturation can cause changes in the emission spectra of tryptophan. Thus, the intrinsic fluorescence of BSA provides considerable information in the study of protein folding and association reactions.[78] The emission spectra of BSA in the presence of different concentrations of **1** were recorded in the wavelength range from 290 to 450 nm with the protein excited at 280 nm. As shown in Figure 12, the addition of the complex to BSA resulted in a significant quenching of emission intensity of ca. 45 % with a slight bathochromic shift ($\Delta\lambda \approx 3$ nm). The quenching of the BSA fluorescence upon the addition of **1** reveals changes to the microenvironment around the tryptophan residue or protein unfolding, both as a result of the BSA interaction with the compound.[79] Moreover, the shift of the emission maxima towards a lower energy indicates a probable energy transfer from the indole unit of the tryptophan to the protein-bound compound.[80]

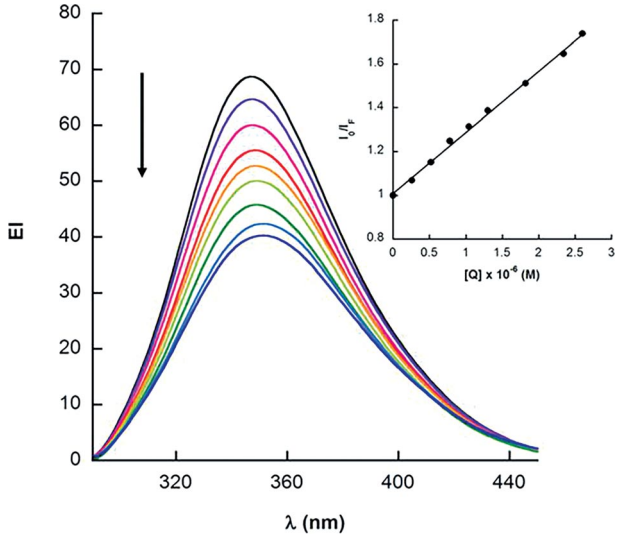

Figure 12. Emission spectra of BSA in absence and presence of 0.26, 0.52, 0.78, 1.0, 1.3, 1.8, 2.3, 2.6×10^{-6} M of **1**; [BSA] = 1.3×10^{-6} M, 0.1 M cacodylate buffer (pH 6.0), and 0.1 % DMF. The arrow shows the changes in intensity at increasing concentrations of the complex. Inset: Stern–Volmer plot.

The fluorescence quenching data were further analyzed by the Stern–Volmer relationship, which can be expressed in terms of the bimolecular quenching rate constant and average lifetime of the fluorophore as shown in Equation (2).[80]

$$I_0/I = 1 + K_{SV}[Q] = 1 + k_q\tau_0[Q] \quad (2)$$

I_0 and I are the fluorescence intensities of the fluorophore in the absence and presence of quencher, K_{SV} is the Stern–Volmer quenching constant, [Q] is the quencher concentration, k_q is the quenching rate constant, and τ_0 is the average lifetime of the biomolecule without quencher (10^{-8} s for BSA).[81]

The plot of I_o/I versus [Q] shows a good linear relationship (inset in Figure 12). The K_{SV} value was found to be 2.79×10^5 M^{-1}, which indicates strong binding between BSA and **1**.[80] A linear Stern–Volmer plot represents a single quenching mechanism, either static or dynamic.[82] Dynamic quenching refers to a process in which the fluorophore and the quencher come into contact during the transient existence of the excited state, whereas static quenching refers to the formation of a fluorophore–quencher complex in the ground state. The calculated bimolecular quenching constant (k_q) for **1** of 2.79×10^{13} M^{-1} s^{-1} is 1000-fold higher than the maximum value for diffusion-controlled quenching (2×10^{10} M^{-1} s^{-1}), which suggests that the quenching mechanism was not initiated by a dynamic quenching but by a static one.[81]

To get further insight into the type of fluorescence quenching performed by **1**, we recorded the UV/Vis absorption spectra of the protein in the absence and presence of **1** (Figure S7). Dynamic quenching only affects the excited states of the fluorophores; therefore, no changes in the absorption spectra are expected upon the addition of the compound. However, the formation of a complex in the ground state generally induces perturbations in the protein structure that produce changes in absorption spectrum of the fluorophore.[83] As shown in Figure S7, the band at $\lambda = 278$ nm in the BSA spectrum showed an increase in the intensity without any shift in wavelength in the presence of the compound. The increase in absorption intensity indicates that more aromatic acid residues (phenyl rings in Trp, Tyr, and Phe) were extended into the aqueous environment.[84] This change, attributed to the formation of a ground-state complex between the compounds and BSA, supports that the quenching process was mainly a static one, as suggested by the k_q value.[81,84] Moreover, the unchanged maximum absorption wavelength implies that the interaction between the complex and BSA is noncovalent in nature. Such an interaction may occur through π–π stacking between the aromatic rings of the ligands in the complexes and the phenyl rings of Trp, Tyr, and Phe residues in the binding cavity of BSA. As these residues possess conjugated π electrons, they are inclined to share electrons with other π systems.[85]

When small molecules bind independently to a set of equivalent sites on a macromolecule, the equilibrium between the free and bound molecules is represented by the Scatchard equation, see Equation (3).

$$\log[(I_0 - I)/I] = \log K_b + n\log[Q] \quad (3)$$

I_0 and I are the fluorescence intensities in the absence and presence of the quencher, respectively, [Q] is the concentration of the quencher, K_b is the binding constant, and n is the number of binding sites. Thus, a plot of $\log[(I_0 - I)/I]$ versus log [Q] can be used to determine the binding constant (from the intercept) and the number of binding sites (from the slope; Fig-

ure S8). The calculated value of *n* of ca. 1 (*n* = 1.01) indicates a single binding site in BSA for **1**. The K_b value (3.32×10^5 M^{-1}) is higher than those found for ternary Cu^{II} complexes with phenanthroline and anti-inflammatory drugs and reveals a strong interaction between the copper(II) complex and BSA.[86]

Conclusions

Herein, the syntheses of two new Cu^{II} complexes, [Cu(QSQ)(phen)]ClO_4·0.5H_2O (**1**) and [Cu(QSQ)(phen)(H_2O)]ClO_4 (**2**), containing the new quinoline sulfonamide derivative *N*-(quinolin-8-yl)quinolin-8-sulfonamide (HQSQ) and phenanthroline are reported. The structures of the complexes were analyzed by X-ray diffraction, which revealed trigonal-bipyramidal geometries around the Cu^{II} centers with a high distortion in **1** and a very slight distortion in **2**. The degree of distortion seems to be imposed by the different coordination behavior of the sulfonamide ligand, which acts as tridentate in **1** and bidentate in **2**. Physicochemical characterization (ESI+ MS, EPR spectroscopy, and UV/Vis spectroscopy) has shown that both complexes give rise to the same entity in solution. Binding-interaction experiments of **1** with CT-DNA and BSA were performed. Complex **1** showed high affinity towards DNA with an apparent binding constant (K_{app}) of 2.45×10^6 M^{-1}. Viscometry measurements indicated that **1** binds to DNA through partial intercalation. Also, the compound showed an intense interaction with BSA (K_b = 3.32×10^5 M^{-1}). Significant fluorescence quenching can be observed when the compound is bound to BSA, and a static quenching mechanism was certified by electronic absorption titrations. Compound **1** efficiently cleaves plasmid pUC18 on photoirradiation as well as with the addition of ascorbate/H_2O_2. Interestingly, **1** is also able to promote DNA cleavage through a self-activating oxidative mechanism involving the generation of superoxide and hydroxyl radicals; therefore, **1** is the first self-activating chemical nuclease among the Cu sulfonamide complexes that have been reported as DNA cleavers. In summary, we have presented a new class of Cu sulfonamide complexes with interesting properties towards DNA (binding affinity, efficient photoinduced and self-activating nuclease activity) that could be the basis for the development of new metal complexes with potential application as DNA-targeted chemotherapeutics.

Experimental Section

Materials and General Methods: $Cu(ClO_4)_2$·6H_2O, other chemicals, and solvents were purchased from Sigma–Aldrich and used without further purification. Calf thymus DNA (CT-DNA, type XV) and pUC18 (0.25 μg/μL) in TE buffer [tris(hydroxymethyl)aminomethane (tris) 10 mM and ethylenediaminetetraacetic acid (EDTA) 1 mM, pH 8.0] were provided by Sigma and Fermentas, respectively. The chemical analyses (C, H, N, S) were performed with a CE Instruments EA 1108 analyzer. The IR spectra were recorded with a Thermo Nicolet iS10 attenuated total reflectance (ATR) FTIR spectrophotometer in the wavenumber range 4000 to 600 cm^{-1}. The ^{1}H and ^{13}C NMR spectra of samples in [D_6]DMSO were recorded with a Bruker Avance DRX-500 spectrophotometer. The chemical shifts are reported in ppm with tetramethylsilane (TMS) as the reference. The UV/Vis spectra of the complexes were recorded with an Agilent 8453 spectrophotometer. The ESI+ MS were recorded with a Bruker Esquire 3000 plus LC–MS system. The X-band EPR spectra were recorded at room temperature with a Bruker ELEXSYS spectrometer, and the X-band EPR spectra of the complexes in DMF were recorded at 40 K.

***N*-(Quinolin-8-yl)quinolin-8-sulfonamide (HQSQ):** The sulfonamide ligand was prepared by mixing 8-aminoquinoline (1 g, 6.9 mmol) with 8-quinolinesulfonyl chloride (2.20 g, 9.7 mmol) in pyridine (7 mL; Scheme 1). The resulting mixture was stirred for 1 h 30 min in an ice bath. Then, it was stirred at room temperature and, cold water (50 mL) was added. The mixture was subsequently stirred for 2 h 30 min in an ice bath. An ochre precipitate was obtained and crystallized from hot ethanol. The solid was then collected by filtration, washed with water, and dried until constant weight (1.98 g, yield 85 %). $C_{18}H_{13}N_3O_2S$ (335.38): calcd. C 64.46, H 3.91, N 12.53, S 9.56; found C 64.32, H 3.97, N 12.52, S 9.45. ^{1}H NMR ([D_6]DMSO, 500 MHz): δ = 10.44 (br s, 1 H, NH), 9.13 (dd, *J* = 4.2, 1.5 Hz, 1 H), 8.83 (dd, *J* = 4.2, 1.5 Hz, 1 H), 8.48 (dd, *J* = 7.3, 1.2 Hz, 1 H), 8.42 (dd, *J* = 8.4, 1.6 Hz, 1 H), 8.23 (td, *J* = 8.4, 1.4 Hz, 2 H), 7.80 (dd, *J* = 7.7, 1.1 Hz, 1 H), 7.72 (t, *J* = 7.8 Hz, 1 H), 7.63 (dd, *J* = 8.3, 4.3 Hz, 1 H), 7.54–7.49 (m, 2 H), 7.43 (t, *J* = 8.0 Hz, 1 H) ppm. ^{13}C NMR ([D_6]DMSO, 125 MHz): δ = 152.0, 149.4, 142.6, 138.2, 137.5, 136.8, 135.0, 134.7, 134.2, 132.2, 128.8, 128.3, 127.2, 126.0, 123.2, 122.8, 122.7, 114.4 ppm. MS (ESI+, DMF): *m/z* = 335.96 [HQSQ + H]$^+$. IR (ATR): $\tilde{\nu}_{max}$ = 3168 [ν(N–H)]; 1593, 1565, 1500 [ν(C=C), ν(C=N)]; 1369 [$\nu_{as}(SO_2)$]; 1145 [$\nu_s(SO_2)$]; 917 [ν(S–N)] cm^{-1}.

[Cu(QSQ)(phen)]ClO_4·0.5H_2O (1) and [Cu(QSQ)(phen)(H_2O)]ClO_4 (2): A solution of $Cu(ClO_4)_2$·6H_2O (92.6 mg, 0.25 mmol) in methanol (30 mL) was added dropwise to a methanolic solution (50 mL) of HQSQ (83.9 mg, 0.25 mmol). The resulting mixture was stirred for 30 min, and then phenanthroline (50.0 mg, 0.25 mmol) was added. The dark green solution was stirred for 2 h and then left to stand at room temperature. Deep green crystals of **1** suitable for X-ray diffraction formed after a few days. The crystals were isolated by filtration, washed with methanol, and dried under vacuum. By the same procedure as that for **1**, blue crystals of **2** were obtained in a small quantity from a methanolic solution containing $Cu(py)_4(ClO_4)_2$ (145.0 mg, 0.25 mmol; py = pyridine), HQSQ (84.0 mg, 0.25 mmol), and phenanthroline (50.0 mg, 0.25 mmol; Scheme 1).

For the synthesis of **2**, $Cu(py)_4(ClO_4)_2$ was previously prepared in a 80 % yield through the addition of pyridine (8 mL, 98 mmol) to an aqueous solution (35 mL) of $Cu(ClO_4)_2$·6H_2O (7.4 g, 20 mmol). The purity of the violet solid obtained was confirmed by elemental analysis. $C_{20}H_{20}Cl_2CuN_4O_8$ (578.85): calcd. C 41.46, H 3.46, N 9.67; found C 41.21, H 3.41, N 9.50.

[Cu(QSQ)(phen)]ClO_4·0.5H_2O (1): Yield 54 %. $C_{30}H_{21}ClCuN_5O_{6.5}S$ (686.56): calcd. C 52.48, H 3.08, N 10.20, S 4.67; found C 52.45, H 3.05, N 10.31, S 4.51. IR (ATR): $\tilde{\nu}_{max}$ = 3522 [ν(O–H)]; 1593, 1579, 1567, 1523, 1504 [ν(C=C), ν(C=N)]; 1313 [$\nu_{as}(SO_2)$]; 1135 [$\nu_s(SO_2)$]; 1074 [$\nu(ClO_4)$]; 950 [ν(S–N)]; 850 [$\nu(C–H)_{phen}$] cm^{-1}. MS (ESI+, DMF/H_2O 20:80): *m/z* = 577.07 [Cu(QSQ)(phen)]$^+$. UV/Vis (DMF): λ_{max} = 480 (sh), 700 (ε = 142 cm^{-1} M^{-1}), 920 (sh) nm.

[Cu(QSQ)(phen)(H_2O)]ClO_4 (2): Yield 5 %. $C_{30}H_{22}ClCuN_5O_7S$ (695.56): calcd. C 51.80, H 3.18, N 10.07, S 4.61; found C 52.12, H 3.16, N 9.97, S 4.45. IR (ATR): $\tilde{\nu}_{max}$ = 3526 [ν(O–H)]; 1593, 1580, 1567, 1522, 1504 [ν(C=C), ν(C=N)]; 1316 [$\nu_{as}(SO_2)$]; 1133 [$\nu_s(SO_2)$]; 1077 [$\nu(ClO_4)$]; 950 [ν(S–N)]; 850 [$\nu(C–H)_{phen}$] cm^{-1}. MS (ESI+, DMF/H_2O 20:80): *m/z* = 577.04 [Cu(QSQ)(phen)]$^+$. UV/Vis (DMF): λ_{max}= 480 (sh), 700 (ε = 149 cm^{-1} M^{-1}), 920 (sh) nm.

Caution! Although no problems were encountered in this work, perchlorate salts are potentially explosive. They should be prepared in small quantities and handled with care.

X-ray Crystallography: Crystals of **1** and **2** were mounted on glass fibers for data collection. The crystal data were collected at room temperature with a Bruker Kappa Apex II diffractometer equipped with a CCD area detector of high sensitivity. The crystal data were measured at room temperature with Cu-K_α radiation (λ = 1.5418 Å). The data were processed with SAINT,[87] and absorption corrections were applied with SADABS.[88] The structures were solved by direct methods and refined by full-matrix least-squares techniques against F^2 with SHELXTL™.[89] Positional and anisotropic atomic displacement parameters were refined for all non-hydrogen atoms. Hydrogen atoms were positioned in geometrically idealized positions and included in a riding model with isotropic displacement parameters constrained to $1.2U_{eq}$ of their carrier atoms. The molecular graphics were generated with SHELXTL™,[89] MERCURY,[90] and ORTEP.[91]

The crystal data, experimental details, and refinement results are summarized in Table S1.

CCDC 1407214 (for **1**) and 1407215 (for **2**) contain the supplementary crystallographic data for this paper. These data can be obtained free of charge from The Cambridge Crystallographic Data Centre.

DNA Binding Studies: DNA melting experiments were performed by monitoring the absorbance of 100 μM CT-DNA at λ = 260 nm at different temperatures in both the absence and presence of **1**. The measurements were performed with an Agilent 8453 UV/Vis spectrophotometer equipped with a Peltier temperature-controlled sample cell and driver (Agilent 89090A). Solutions containing the ternary complex **1** and CT-DNA in phosphate buffer (pH 7.2, 1 mM phosphate, 2 mM NaCl) and 2.5 % DMF were stirred continuously and heated with a temperature increase rate of 1 °C min^{-1}. The temperature interval studied ranged from 25 to 90 °C. The melting point was obtained from the first derivative by using the Savitsky–Golay algorithm. The fluorescence spectra were recorded with a JASCO FP-6200 spectrofluorimeter. The experiments entailed the addition of copper(II) complex solutions at final concentrations of 0 to 180 μM to samples containing 50 μM CT-DNA (bp) and 50 μM ethidium bromide in cacodylate buffer (0.1 M, pH 6.0) and 3.5 % DMF. The samples were excited at λ = 500 nm, and the emission was recorded between λ = 530 and 680 nm. The nonlinear least-squares analyses were performed with KaleidaGraph version 4.0. Viscosity experiments were performed with a semi-micro Ubbelodhe viscometer immersed in a Julabo ME16G thermostatted bath maintained at 25.0 ± 0.1 °C. Solutions of **1** (with final concentrations of 1 to 10 μM) in 0.1 M cacodylate buffer (pH 6.0) and 2 % DMF were added to a solution of CT-DNA (50 μM bp) in cacodylate buffer (0.1 M, pH 6.0). The flow times were measured in triplicate with a stopwatch. The data were presented as $(\eta/\eta_0)^{1/3}$ versus the ratio of the complex concentration to DNA; η is the viscosity of DNA in the presence of the complex, and η_0 is the viscosity of DNA alone. The viscosity values were calculated from the observed flow time of a solution containing DNA corrected for the flow time of buffer alone (t_0), $\eta = t - t_0$. The cyclic voltammetry experiments were performed in a single-compartment cell with a three-electrode system and a PAR 273A potentiostat. The working and auxiliary electrodes were platinum, and the reference electrode was Ag/AgCl (satd. KCl). The solvent was DMF, and the supporting electrolyte was tetrabutylammonium perchlorate. DMF solutions (0.1 M) of the complex in the absence and presence of CT-DNA ([complex]/[DNA] = 10 and 20) were deoxygenated by purging with nitrogen for 15 min before the measurements.

Nuclease Activity: The reactions were performed with pUC18 and **1** in 0.1 M cacodylate buffer at pH 6.0. The complex solution was initially prepared in DMF and then diluted with cacodylate buffer. The samples were prepared by mixing pUC18 (0.5 μL, 0.50 μg/μL) with the complex solution (3 μL) at increasing concentrations and diluted with cacodylate buffer (0.1 M, pH 6.0) to a total volume of 20 μL. The final solutions contained 5 % DMF. For the photoinduced cleavage studies, the reactions were illuminated with UV-A lamps at 365 nm (Luzchem Research, Inc.). Samples in Eppendorf vials were photoexposed for 2 h. Then, the samples were incubated for 2 h at 37 °C in the dark. A loading buffer (4 μL; 0.25 % bromophenol blue, 0.25 % xylene cyanol, and 30 % glycerol) was added to the samples, which were finally loaded on a 0.8 % agarose gel in 0.5 × TBE buffer (0.045 M tris, 0.045 M boric acid, and 1 mM EDTA) containing ethidium bromide (2 μL/100 mL; 10 mg/mL). The electrophoresis was performed in the dark at 80 V for 2 h. The gels were photographed with a UVITEC Cambridge-UVIDOC HD2 gel imaging system. The relative amounts of different plasmid forms were quantified with the aid of ImageJ 1.3s.[92] A correction factor of 1.31 was used for the assessment of supercoiled DNA (Form I) as the intercalation between EB and form I DNA is relatively weak compared with those of form II (nicked) and form III (linear) DNA.[93]

In the cleavage assays without external agents, samples containing pUC18 and the compound at increasing concentrations were incubated for 2 h in the dark at 37 °C. For the cleavage studies in the presence of activating agent, ascorbate/H_2O_2 in cacodylate buffer was added at an equimolar concentration to the reaction mixtures, which were incubated for 1 h at 37 °C. After incubation, samples without activating agent and with ascorbate/H_2O_2 were treated as described above for the photocleavage experiments.

To test for the presence of ROS generated during strand scission and for possible complex–DNA interaction sites, various reactive oxygen intermediate scavengers (TMPP, DABCO, tiron, sodium formate, potassium iodide, and DMSO) and groove binders (methyl green and Hoechst 33258) were added to the pUC18 solution before complex addition in all of the different nuclease assays. For the D_2O experiment, this solvent was used for dilution of the sample solution to a volume of 20 μL. Moreover, a chelating agent of copper(I), neocuproine, was also assayed.

BSA Binding Studies: A stock solution of BSA (5.0×10^{-4} M) was prepared in cacodylate buffer (0.1 M, pH 6.0) and stored at 4 °C in the dark for a maximum time of 2 d. A concentrated stock solution of **1** (5×10^{-3} M) was prepared in DMF and diluted suitably with cacodylate buffer to the required concentration. A BSA solution (1.3×10^{-6} M, 3 mL) was titrated by successive additions of the complex solution to give final concentrations of 0.26×10^{-6} to 2.6×10^{-6} M. The final samples contained 0.1 % DMF. For every addition, the mixture was allowed to stand for 20 min at room temperature. The samples were excited at λ = 280 nm, and emission was recorded at λ = 290–450 nm. The UV/Vis spectra of BSA in the absence and presence of the Cu^{II} compound were recorded at room temperature. The samples were prepared in 0.1 M cacodylate buffer (pH 6.0) and 0.25 % DMF. To correct the absorbance of **1** itself, the UV spectrum of **1** alone was recorded under the same experimental conditions and subtracted from that of BSA plus compound.

Supporting Information (see footnote on the first page of this article): Crystal data, perspective view of π–π interactions, EPR spectra, UV/Vis spectra, agarose gel electrophoresis, UV/Vis spectra of BSA and BSA+**1**, plot of $\log[(I_0 - I)/I]$ versus log [Q].

Acknowledgments

The authors acknowledge the financial support from the Spanish Comisión Interministerial de Ciencia y Tecnología (CTQ2007-63690).

Keywords: Copper · DNA binding · DNA cleavage · Protein binding · Antitumor agents · Medicinal chemistry

[1] J. Chen, J. Stubbe, *Nat. Rev. Cancer* **2005**, *5*, 102–112.
[2] F. Mancin, P. Scrimin, P. Tecilla, U. Tonellato, *Chem. Commun.* **2005**, 2540–2548.
[3] I. Romero-Canelón, P. J. Sadler, *Inorg. Chem.* **2013**, *52*, 12276–12291.
[4] D. S. Sigman, D. R. Graham, V. D. Aurora, A. M. Stern, *J. Biol. Chem.* **1979**, *254*, 12269–12272.
[5] L. Li, K. Du, Y. Wang, H. Jia, X. Hou, H. Chao, L. Ji, *Dalton Trans.* **2013**, *42*, 11576–11588.
[6] S. M. Hadi, M. F. Ullah, U. Shamim, S. H. Bhat, A. S. Azmi, *Chemotherapy* **2010**, *56*, 280–284.
[7] R. Bonnett, *Chemical Aspects of Photodynamic Therapy*, Gordon and Breach, London, **2000**.
[8] M. R. Detty, S. L. Gibson, S. J. Wagner, *J. Med. Chem.* **2004**, *47*, 3897–3915.
[9] B. W. Henderson, T. M. Busch, L. A. Vaughan, N. P. Frawley, D. Babich, T. A. Sosa, J. D. Zollo, A. S. Dee, M. T. Cooper, D. A. Bellnier, W. R. Greco, A. R. Oseroff, *Cancer Res.* **2000**, *60*, 525–529.
[10] Y. N. Konan, R. Gurny, E. Allémann, *J. Photochem. Photobiol. B* **2002**, *66*, 89–106.
[11] R. Bonnett, *J. Heterocycl. Chem.* **2002**, *39*, 455–470.
[12] J. F. Lovell, T. W. B. Liu, J. Chen, G. Zheng, *Chem. Rev.* **2010**, *110*, 2839–2857.
[13] M. Ethirajan, Y. Chen, P. Joshi, R. K. Pandey, *Chem. Soc. Rev.* **2011**, *40*, 340–362.
[14] S. L. H. Higgins, K. J. Brewer, *Angew. Chem. Int. Ed.* **2012**, *51*, 11420–11422; *Angew. Chem.* **2012**, *124*, 11584.
[15] K. E. Erkkila, D. T. Odom, J. K. Barton, *Chem. Rev.* **1999**, *99*, 2777–2795.
[16] A. K. Patra, S. Dhar, M. Nethaji, A. R. Chakravarty, *Chem. Commun.* **2003**, 1562–1563.
[17] S. Dhar, D. Senapati, P. K. Das, P. Chattopadhyay, M. Nethaji, A. R. Chakravarty, *J. Am. Chem. Soc.* **2003**, *125*, 12118–12124.
[18] S. Dhar, A. R. Chakravarty, *Inorg. Chem.* **2005**, *44*, 2582–2584.
[19] U. Schatzschneider, *Eur. J. Inorg. Chem.* **2010**, 1451–1467.
[20] K. Suntharalingam, D. J. Hunt, A. A. Duarte, A. J. P. White, D. J. Mann, R. Vilar, *Chem. Eur. J.* **2012**, *18*, 15133–15141.
[21] B. Zheng, C. Wang, X. Xin, F. Liu, X. Zhou, J. Zhang, S. Guo, *J. Phys. Chem. C* **2014**, *118*, 7637–7642.
[22] D. Lahiri, T. Bhowmick, B. Pathak, O. Shameema, A. K. Patra, S. Ramakumar, A. R. Chakravarty, *Inorg. Chem.* **2009**, *48*, 339–349.
[23] S. S. Tonde, A. S. Kumbhar, S. B. Padhye, R. J. Butcher, *J. Inorg. Biochem.* **2006**, *100*, 51–57.
[24] A. Kellett, M. O'Connor, M. McCann, M. McNamara, P. Lynch, G. Rosair, V. McKee, B. Creaven, M. Walsh, S. McClean, A. Foltyn, D. O'Shea, O. Howe, M. Devereux, *Dalton Trans.* **2011**, *40*, 1024–1027.
[25] P. U. Maheswari, S. Roy, H. den Dulk, S. Barends, G. P. van Wezel, B. Kozlevcár, P. Gamez, J. Reedijk, *J. Am. Chem. Soc.* **2006**, *128*, 710–711.
[26] P. U. Maheswari, M. van der Ster, S. Smulders, S. Barends, G. P. van Wezel, C. Massera, S. Roy, H. den Dulk, P. Gamez, J. Reedijk, *Inorg. Chem.* **2008**, *47*, 3719–3727.
[27] K. Li, L. H. Zhou, J. Zhang, S. Y. Chen, Z. W. Zhang, J. J. Zhang, H. H. Lin, X. Q. Yu, *Eur. J. Med. Chem.* **2009**, *44*, 1768–1772.
[28] E. Lamour, S. Routier, J. L. Bernier, J. P. Catteau, C. Bailly, H. Vezin, *J. Am. Chem. Soc.* **1999**, *121*, 1862–1869.
[29] K. Ghosh, P. Kumar, N. Tyagi, U. P. Singh, V. Aggarwal, M. C. Baratto, *Eur. J. Med. Chem.* **2010**, *45*, 3770–3779.
[30] K. Ghosh, P. Kumar, N. Tyagi, U. P. Singh, N. Goel, *Inorg. Chem. Commun.* **2011**, *14*, 489–492.
[31] K. Ghosh, P. Kumar, V. Mohan, U. P. Singh, S. Kasiri, S. S. Mandal, *Inorg. Chem.* **2012**, *51*, 3343–3345.
[32] D. C. Carter, J. X. Ho, *Adv. Protein Chem.* **1994**, *45*, 153–176.
[33] Y.-Z. Zhang, J. Dai, X. Xiang, W.-W. Li, Y. Liu, *Mol. Biol. Rep.* **2010**, *37*, 1541–1549.
[34] M. Ganeshpandian, R. Loganathan, S. Ramakrishnan, A. Riyasdeen, M. A. Akbarsha, M. Palaniandavar, *Polyhedron* **2013**, *52*, 924–938.
[35] T. H. Maren, C. W. Conroy, *J. Biol. Chem.* **1993**, *268*, 26233–26239.
[36] A. Scozzafava, T. Owa, A. Mastrolorenzo, C. T. Supuran, *Curr. Med. Chem.* **2003**, *10*, 925–953.
[37] T. Owa, H. Toshino, T. Okauchi, K. Yoshimatsu, Y. Ozawa, N. H. Sugi, T. Nagasu, N. Koyanagi, K. Kitoh, *J. Med. Chem.* **1999**, *42*, 3789–3799.
[38] N. Koyanagi, T. Nagasu, F. Fujita, T. Watanabe, K. Tsukahara, Y. Funahashi, M. Fujita, T. Taguchi, H. Yoshino, K. Kitoh, *Cancer Res.* **1994**, *54*, 1702–1706.
[39] A. K. Ghosh, L. M. Swanson, H. Cho, S. Leshchenko, K. A. Hussain, S. Kay, D. E. Walters, Y. Koh, H. Mitsuya, *J. Med. Chem.* **2005**, *48*, 3576–3585.
[40] F. Zhong, G. Geng, B. Chen, T. Pan, Q. Li, H. Zhang, C. Bai, *Org. Biomol. Chem.* **2015**, *13*, 1792–1799.
[41] Y. Ozawa, N. H. Sugi, T. Nagasu, T. Owa, T. Watanabe, N. Koyanagi, H. Yoshino, K. Kitoh, K. Yoshimatsu, *Eur. J. Cancer* **2001**, *37*, 2275–2282.
[42] K. Fukuoka, J. Usuda, Y. Iwamoto, H. Fukumoto, T. Nakamura, T. Yoneda, N. Narita, N. Saijo, K. Nishio, *Invest. New Drugs* **2001**, *19*, 219–227.
[43] G. Laconde, N. Pommery, P. Depreux, P. Berthelot, J. P. Henichart, *J. Enzyme Inhib. Med. Chem.* **2003**, *18*, 89–94.
[44] R. Mohan, M. Banerjee, A. Ray, T. Manna, L. Wilson, T. Owa, B. Bhattacharyya, D. Panda, *Biochemistry* **2006**, *45*, 5440–5449.
[45] J. F. Smyth, S. Aaamdal, A. Awada, C. Dittrich, F. Caponigro, P. Schoffski, M. Gore, T. Lesimple, N. Djurasinovic, B. Baron, M. Ravic, P. Fumoleau, C. Punt, *Ann. Oncol.* **2005**, *16*, 158–161.
[46] M. M. Ghorab, F. A. Ragab, H. I. Heiba, R. K. Arafa, E. M. El-Hossary, *Eur. J. Med. Chem.* **2010**, *45*, 3677–3684.
[47] Y. H. Kim, K. J. Shin, T. G. Lee, E. Kim, M. S. Lee, S. H. Ryu, P. G. Suh, *Biochem. Pharmacol.* **2005**, *69*, 1333–1341.
[48] J. L. García-Giménez, J. Hernández-Gil, A. Martínez-Ruíz, A. Castiñeiras, M. Liu-González, F. V. Pallardó, J. Borrás, G. Alzuet-Piña, *J. Inorg. Biochem.* **2013**, *121*, 167–178.
[49] M. González-Álvarez, A. Pascual-Álvarez, L. del Castillo Agudo, A. Castiñeiras, M. Liu-González, J. Borrás, G. Alzuet-Piña, *Dalton Trans.* **2013**, *42*, 10244–10259.
[50] J. L. García-Giménez, M. González-Álvarez, M. Liu-González, B. Macías, J. Borrás, G. Alzuet, *J. Inorg. Biochem.* **2009**, *103*, 923–934.
[51] J. L. García-Giménez, G. Alzuet, M. González-Álvarez, M. Liu-González, A. Castiñeiras, J. Borrás, *J. Inorg. Biochem.* **2009**, *103*, 243–255.
[52] M. González-Álvarez, G. Alzuet, J. Borrás, L. del Castillo-Agudo, J. M. Montejo-Bernardo, A. Gutiérrez-Rodríguez, S. García-Granda, *J. Biol. Inorg. Chem.* **2008**, *13*, 1249–1265.
[53] J. L. García-Giménez, G. Alzuet, M. González-Álvarez, A. Castiñeiras, M. Liu-González, J. Borrás, *Inorg. Chem.* **2007**, *46*, 7178–7188.
[54] M. González-Álvarez, G. Alzuet, L. del Castillo, J. Borrás, M. Liu-González, *Eur. J. Inorg. Chem.* **2006**, 3823–3834.
[55] R. Cejudo, G. Alzuet, M. González-Álvarez, J. L. García-Gimenez, J. Borrás, M. Liu-González, *J. Inorg. Biochem.* **2006**, *100*, 70–79.
[56] M. González-Álvarez, G. Alzuet, J. Borrás, B. Macías, A. Castiñeiras, *Inorg. Chem.* **2003**, *42*, 2992–2998.
[57] M. González-Álvarez, G. Alzuet, J. Borrás, M. Pitié, B. Meunier, *J. Biol. Inorg. Chem.* **2003**, *8*, 644–652.
[58] A. W. Addison, T. N. Rao, J. Reedijk, J. van Rijn, C. G. Verschoor, *J. Chem. Soc., Dalton Trans.* **1984**, 1349–1356.
[59] C. Deraeve, A. Maraval, L. Vendier, V. Faugeroux, M. Pitié, B. Meunier, *Eur. J. Inorg. Chem.* **2008**, 5622–5631.
[60] J. Yang, J. F. Ma, D. M. Wu, L. P. Guo, J. F. Liu, *J. Mol. Struct.* **2003**, *657*, 333–341.
[61] K. Nakamoto, *Infrared and Raman Spectra of Inorganic and Coordination Compounds*, 4th ed., Wiley, New York, **1986**, p. 253.
[62] *WINEPR-Simfonia*, v. 1.25, Bruker Analytik, Karlsruhe, Germany, **1994**–**1996**.
[63] A. Kunishita, M. Kubo, H. Ishimaru, T. Ogura, H. Sugimoto, S. Itoh, *Inorg. Chem.* **2008**, *47*, 12032–12039.
[64] I. Bertini, in: *ESR and NMR of Paramagnetic Species in Biological and Related Systems* (Eds.: I. Bertini, R. S. Drago), Reidel, Dordrecht, The Netherlands, **1980**, chapter 9, p. 214–215.
[65] P. Nagle, E. O'Sullivan, B. J. Hathaway, E. Muller, *J. Chem. Soc., Dalton Trans.* **1990**, 3399–3406.
[66] R. Uma, R. Viswanathan, M. Palaniandavar, M. Lakshminarayanan, *J. Chem. Soc., Dalton Trans.* **1994**, 1219–1226.
[67] E. T. Tselepi-Kalouli, N. Katsaros, *J. Inorg. Biochem.* **1989**, *37*, 271–282.
[68] S. Dhar, M. Nethaji, A. R. Chakravarty, *Inorg. Chem.* **2005**, *44*, 8876–8883.

[69] B. C. Baguley, M. Le Bret, *Biochemistry* **1984**, *23*, 937–943.
[70] B. Selvakumar, V. Rajendiran, P. Uma, H. Maheswari, M. Stoeckli-Evans, J. Palaniandavar, *J. Inorg. Biochem.* **2006**, *100*, 316–330.
[71] C. J. Murphy, M. R. Arkin, N. D. Ghatlia, S. Bossmann, N. J. Turro, J. K. Barton, *Proc. Natl. Acad. Sci. USA* **1994**, *91*, 5315–5319.
[72] J. Shao, W. G. Bao, H. Tian, B. Li, X. F. Zhao, X. Qiao, J.-Y. Xu, *Dalton Trans.* **2014**, *43*, 1663–1671.
[73] X. Sheng, X. Guo, X.-M. Lu, G. Y. Lu, Y. Shao, F. Liu, Q. Xu, *Bioconjugate Chem.* **2008**, *19*, 490–498.
[74] C. Tolia, A. N. Papadopoulos, C. P. Raptopoulou, V. Psycharis, C. Garino, L. Salassa, G. Psomas, *J. Inorg. Biochem.* **2013**, *123*, 53–65.
[75] M. Sirajuddin, S. Ali, A. Badshah, *J. Photochem. Photobiol. B* **2013**, *124*, 1–19.
[76] K. Szaciłowski, W. Macyk, A. Drzewiecka-Matuszek, M. Brindell, G. Stochel, *Chem. Rev.* **2005**, *105*, 2647–2694.
[77] P. Krishnamoorthy, P. Sathyadevi, A. H. Cowley, R. R. Butorac, N. Dharmaraj, *Eur. J. Med. Chem.* **2011**, *46*, 3376–3387.
[78] J. Lu, Q. Sun, J. L. Li, L. Jiang, W. Gu, X. Liu, J. L. Tian, S. P. Yan, *J. Inorg. Biochem.* **2014**, *137*, 46–56.
[79] Y. Ni, R. Zhu, S. Kokot, *Analyst* **2011**, *136*, 4794–4801.
[80] M. Das, R. Nasani, M. Saha, S. M. Mobin, S. Mukhopadhyay, *Dalton Trans.* **2015**, *44*, 2299–2310.
[81] C. Y. Gao, X. Qiao, Z. Y. Ma, Z. G. Wang, J. Lu, J. L. Tian, J. Y. Xu, S. P. Yan, *Dalton Trans.* **2012**, *41*, 12220–12232.
[82] M. R. Eftink, C. A. Ghiron, *J. Phys. Chem.* **1976**, *80*, 486–493.
[83] E. Ramachandran, D. S. Raja, J. L. Mike, T. R. Wagner, M. Zeller, K. Natarajan, *RSC Adv.* **2012**, *2*, 8515–8525.
[84] F. Samari, B. Hemmateenejad, M. Shamsipur, M. Rashidi, H. Samouei, *Inorg. Chem.* **2012**, *51*, 3454–3464.
[85] Y. Wang, X. Wang, J. Wang, Y. Zhao, W. He, Z. Guo, *Inorg. Chem.* **2011**, *50*, 12661–12668.
[86] F. Dimiza, F. Perdih, V. Tangoulis, I. Turel, D. P. Kessissoglou, G. Psomas, *J. Inorg. Biochem.* **2011**, *105*, 476–489.
[87] *SAINT – Data Reduction Program*, v. 7.68A, Bruker AXS Inc., Madison, WI, USA, **2006**.
[88] *SADABS – Empirical Absorption Program*, v. 2.03, Bruker AXS Inc., Madison, WI, USA, **2006**.
[89] G. M. Sheldrick, *SHELXTL™ – Structure Determination Software Suite*, v. 6.14, Bruker AXS Inc., Madison, WI, USA, **2003**.
[90] *MERCURY Molecular Graphics*, v. 3.0: C. F. Macrae, P. R. Edgington, P. McCabe, E. Pidcock, G. P. Shields, R. Taylor, M. Towler, J. van de Streek, *J. Appl. Crystallogr.* **2006**, *39*, 453–457.
[91] *ORTEP3 for Windows*: L. J. Farrugia, *J. Appl. Crystallogr.* **1997**, *30*, 565–566.
[92] W. Rasband, *ImageJ 1.34s*, *National Institutes of Health*, USA, **2008**.
[93] R. P. Hertzberg, *J. Am. Chem. Soc.* **1982**, *104*, 313–315.

Received: December 21, 2015
Published Online: February 4, 2016